Environmental Science Nano

ROYAL SOCIETY OF CHEMISTRY

PAPER

View Article Online
View Journal | View Issue

Cite this: *Environ. Sci.: Nano*, 2025, **12**, 1477

Adaptive responses of *Bacillus subtilis* underlie differential nanoplastic toxicity with implications for root colonization†

Franklin Perez,[a] Nesha May O. Andoy,[a] Uyan Tran Thao Hua,[a] Keiko Yoshioka[bc] and Ruby May A. Sullan *[ad]

Positively charged nanoplastics are more toxic to microorganisms than their negatively charged counterparts, prompting further investigation into their antimicrobial properties. While many studies have shown that positively charged nanoplastics bind to bacteria, the fate of these nanoplastic coatings during bacterial growth remains unclear. Here, we report how amine-modified polystyrene nanoplastics (PS-NH_2) reduce the viability of the plant growth-promoting rhizobacterium *Bacillus subtilis* and impair its ability to colonize plant roots. We found that upon exposure to PS-NH_2, the nanoplastics form stable, multilayer coatings on the surface of the bacteria. In response, *B. subtilis* initiates processes to remove these nanoplastics—a behavior heavily influenced by their growth environment, whether at air or liquid interfaces. Consequently, we observed differential toxicity under varying growth conditions. Using tomato plant as a model system, we found that these nanoplastics severely inhibit bacterial attachment to plant roots. Our results demonstrate that nanoplastics can disrupt beneficial interactions between soil bacteria and plants, potentially compromising the effectiveness of microbial biofertilizers. Given that current practices introduce large amounts of plastics into agricultural areas, the adverse effects of nanoplastic pollution need to be mitigated.

Received 6th October 2024,
Accepted 16th December 2024

DOI: 10.1039/d4en00936c

rsc.li/es-nano

Environmental significance

Nanoplastics in agricultural soils pose significant risks by harming beneficial soil bacteria essential for soil fertility and sustainable agriculture. Our study provides direct evidence that positively charged nanoplastics form stable, multilayer coatings on a plant growth-promoting rhizobacteria and severely impairs its ability to colonize plant roots. By demonstrating how nanoplastics negatively impact these beneficial relationships, we highlight the potential for nanoplastic pollution to contribute to declining soil fertility. We also found that growing bacteria in liquid environments may mitigate the adverse effects of nanoplastics that bind strongly to bacterial surfaces, suggesting possible strategies to protect soil microbial health. This study emphasizes the urgent need to understand the impact of nanoplastics on soil ecosystems to safeguard agricultural productivity and ecosystem function.

Introduction

Global trends project that there will be ~12 000 million metric tons of plastics in the environment by the year 2050.[1] While the potential risks of plastic pollution in aquatic ecosystems have garnered more attention, evidence suggests that land-based environments may contain larger quantities of plastics than previously recognized.[2,3] Specifically, agricultural soils, which are the bedrock of food production, are tainted with hazardous plastic materials, including abraded tires, biosolids, and plastic mulch films which are excessively used in current agricultural practices.[4] Over 40% of these materials are not recovered and can therefore degrade over time to smaller plastics, forming microplastics (~1–5 μm) and eventually nanoplastics (<1 μm).[5,6]

[a] *Department of Physical and Environmental Sciences, University of Toronto Scarborough, 1065 Military Trail, Toronto, ON, M1C 1A4, Canada. E-mail: ruby.sullan@utoronto.ca*
[b] *Department of Cell and Systems Biology, University of Toronto, 25 Wilcocks St, Toronto, ON, M5S 3B2, Canada*
[c] *Center for the Analysis of Genome Evolution and Function, University of Toronto, 25 Wilcocks St, Toronto, ON, M5S 3B2, Canada*
[d] *Department of Chemistry, University of Toronto, 80 St. George St, Toronto, ON, M5S3H6, Canada*

† Electronic supplementary information (ESI) available: Additional data on bacterial growth curves, characterization of nanoplastics using dynamic light scattering (DLS) and TEM, additional AFM and TEM images on nanoplastic–*B. subtilis* interaction, as well SEM images of *B. subtilis* on different regions of the tomato root. See DOI: https://doi.org/10.1039/d4en00936c

The smaller-sized nanoplastics, with their larger surface area-to-volume ratios, pose a greater hazard due to higher reactivity.[5,7,8] Nanoplastics have been observed to negatively impact microorganisms, as well as invertebrates and plants within soil biota, jeopardizing soil ecosystem functionality and the sustainability of food production systems.[9–12] Of particular interest in agricultural soil is the impact of nanoplastic pollution on the rhizosphere.[10,11,13] While most studies highlight the negative impacts of nanoplastic exposure, one notable work reported that plant growth-promoting rhizobacteria (PGPR) can utilize the polystyrene nanoplastics, suggesting potential use of PGPR for bioremediation of plastic pollution.[14] The rhizosphere is important in sustainable agriculture, serving as a zone where plant roots interact with soil microorganisms. One example of a soil-dwelling rhizobacterium that symbiotically interacts with plant roots is *Bacillus subtilis*. This bacterium heavily relies on the successful colonization of roots *via* biofilm formation in order to promote plant growth and protection from pathogens through the induced systemic resistance.[15] For instance, *B. subtilis* has shown distinct chemotactic behavior towards the root elongation zone of *Arabidopsis thaliana*.[16] In the case of lettuce plants, *Lactuca sativa*, *B. subtilis* displayed preferential attachment to the root cap before colonizing other areas of the root.[17]

In addition to being a beneficial terrestrial bacterium, *B. subtilis* can also grow and form three types of biofilms *in vitro*: (i) colony biofilms at air–solid interface, (ii) pellicle biofilms at air–liquid interface, and (ii) submerged surface-attached biofilms at solid–liquid interface.[15] The various modes of biofilm growth enable this bacterium to adapt to different environmental conditions, making *B. subtilis* an ideal model for studying how rhizobacteria respond to nanoplastic pollution, which is a looming environmental problem.

Here, we monitored the fate of nanoplastics bound to the surface of *B. subtilis* under different growth conditions. Using positively charged polystyrene (PS-NH_2) nanobeads as a model nanoplastic material, we demonstrate that *B. subtilis* activates mechanisms to remove bound nanoplastics from its surface before resuming cell division. However, at overwhelming nanoplastic concentrations, this active bacterial response—coupled with the ability of PS-NH_2 to form multilayered, highly stable nanoplastic coatings—contributes to the bactericidal effects of PS-NH_2. We further demonstrate that this adaptive response underlies the differential toxicity observed between air–agar and liquid interfaces, markedly inhibiting the ability of *B. subtilis* to form biofilms under semi-dry conditions. Consequently, nanoplastic-coated bacteria exhibit severely impaired root colonization.

Methods

Characterization of polystyrene (PS) nanoplastics

Unmodified PS (100 nm), fluorescent amine (PS-NH_2, 100 nm, with an excitation (ex) wavelength of 481 nm and emission (em) wavelength of 540 nm), fluorescent sulfate (PS-SO_4, 100 nm, ex: 538 nm, em: 584 nm), and fluorescent carboxylate (PS-COO^-, 30 nm, ex: 470 nm, em: 505 nm) nanobeads were purchased from Sigma-Aldrich and stored at 4 °C until use. Prior to each experiment, the commercial solution was dialyzed against MilliQ water using a dialysis tubing (14 kDa weight cellulose membrane, 10 mm flat width, Sigma Aldrich) and placed in a covered 2 L beaker to remove preservatives.[18] The concentration of nanoplastics after dialysis was determined using a UV-VIS spectrometer (Cary 60, Agilent Technologies). Particle diameters were measured using dynamic light scattering (DLS, NanoBrook Omni, Brookhaven Instruments), and surface zeta potential was determined using phase analysis light scattering (PALS, NanoBrook Omni, Brookhaven Instruments). Nanoplastic morphology was characterized using transmission electron microscopy (TEM, Hitachi H7500, MegaView III, Olympus, USA). Results of our nanoplastic characterization are summarized in Fig. S1.†

Bacterial growth with nanoplastics

Bacillus subtilis (ATCC© 6051™) was obtained from the American Type Culture Collection. To assess the effects of nanoplastic exposure, a single colony was first cultured in Luria Bertani/Lennox broth (10 g L^{-1} tryptone, 5 g L^{-1} NaCl, 5 g L^{-1} yeast extract, pH 6.9, Sigma-Aldrich) at 37 °C with shaking at 250 rpm for 5 h. Bacterial pellet was then collected through centrifugation at 4000 rpm for 5 min at 4 °C (centrifuge 5804 R, Eppendorf), then washed with nanopure water 3×. Bacterial suspension in water (OD = 0.01) was then exposed to increasing concentrations of nanoplastics (0–20 μg mL^{-1}), covered with aluminum foil, and mixed for 30 minutes using a 20 rpm rotator at room temperature. Subsequently, 5 μL from each microtube was mixed with 195 μL of fresh LB in a pre-sterilized U-shaped 96-well plate, and OD_{600} measurements were recorded every 15 min for 15 hours. The microplate reader (Infinite® 200 Pro, TECAN) provided orbital shaking at 2.5 mm and maintained a temperature of 37 °C. Replicates were obtained from three microplate trials, each using a different colony. Maximum growth, growth rate and lag phase were obtained from Gompertz fit analysis of growth curves and one-way ANOVA was used for statistical analysis.

Atomic force microscopy (AFM) characterization

B. subtilis with and without PS-NH_2 exposure were prepared as described above. After incubation with PS-NH_2, the bacteria–nanoplastic suspensions were filtered onto polyethyleneimine (PEI)-coated polycarbonate (PC) membranes (25 mm diameter, 0.1 μm pore size, Millipore, Oakville, ON, Canada) to immobilize the bacteria for AFM imaging. The PEI-coated PC membranes were prepared by incubating PC membranes in a 1% PEI solution in water overnight at 23 °C with shaking at 60 rpm. The PEI-coated membranes were washed extensively with MilliQ water before use. The PC membrane-immobilized *B. subtilis* were then imaged directly using AFM to characterize the extent of nanoplastic binding with increasing PS-NH_2

concentrations. To monitor the fate of nanoplastics bound to the cell surface during growth, *B. subtilis* that were pre-exposed to 2.5 μg mL^{-1} of PS-NH_2 were immobilized on PC membranes and then incubated at 37 °C under two conditions: (1) submerged in LB media for 3 and 5 hours, and (2) placed at the air–agar interface (on LB agar) for 12 h. After the specified incubation periods, the membranes were washed with PBS and fixed using 1% glutaraldehyde for 2 h at RT. AFM imaging was done using the quantitative imaging (QI) mode of a Nanowizard 4 AFM (JPK Instruments, Berlin, Germany) using silicon nitride probes (SNL-A, Bruker). QI force–distance curves were recorded with a relative force setpoint of 1 nN, a *z*-range of 1000 nm, and a vertical cantilever speed of 100 μm s^{-1}. Unless otherwise stated, measurements were performed at ~25 °C using MilliQ as the imaging solution. For bacteria grown on air–agar interface, ~4–5 bacteria were imaged for each of the $n = 2$ replicates. For other conditions (*i.e.*, immediately after pre-exposure to PS-NH_2 and nanoplastic-coated bacteria grown under liquid LB media), ~15–20 bacteria were imaged for each of the $n \geq 3$ replicates.

Transmission electron microscopy (TEM) of bacteria and nanoplastic

Mid-exponential phase *B. subtilis* were harvested by centrifugation at 4000 rpm and 4 °C for 5 minutes (repeated 3×). Between each centrifugation, the pellets were washed and resuspended in MilliQ water. The cells were then diluted to a final OD_{600} = 0.2 and mixed with PS-NH_2 at final concentrations of 0, 50, 100, 200, and 400 μg mL^{-1} in MilliQ water. Maintaining a bacterial suspension at OD_{600} = 0.2 ensured a constant bacteria-to-nanoplastic ratio, which is crucial because a 20-fold increase in nanoplastic concentration is required for TEM sample preparation, and this ratio significantly influences the inhibitory effects of nanoplastic exposure. Samples were placed on a 20 rpm rotator for 30 min at room temperature in the dark. After centrifugation, bacterial pellets were then collected at 4000 rpm for 10 min at 4 °C. The supernatant was removed, and the pellets were fixed with 2.5% glutaraldehyde for 1 hour at room temperature. Following fixation, the pellets were washed 3× with MilliQ water and stored overnight until sample processing, which involved a series of ethanol dehydrations, uranyl acetate staining, and resin embedding. During imaging, at least 50 cells were imaged per nanoplastic concentration.

Impact of nanoplastics toward agar–air biofilms

B. subtilis cells were harvested by centrifugation at 4000 rpm and 4 °C for 5 min, then washed 3× with MilliQ water. The cells were then diluted to a final OD_{600} = 0.01 in MilliQ water containing PS-NH_2 at final concentrations of 0, 2.5, 5, 10, 12.5, 15 and 20 μg mL^{-1}, all prepared in 1.8 mL microtubes. The microtubes were placed on a rotator at 20 rpm for 30 min at room temperature in the dark, covered with aluminum foil. After incubation, 10 μL aliquots were spotted onto LB or LBGM agar plates, which were kept incubated (static) at 30 °C and monitored for growth over 1 and 5 days. Three replicates were performed per condition and images were acquired using an iPhone 7 camera.

Impact of nanoplastics toward biofilm formation on tomato roots

Tomato seeds were placed on half-strength Murashige and Skoog (1/2 MS) agar and incubated in the dark for 2 days followed by 3 days of light at room temperature. To prevent water from collecting on the plant roots, agar plates were kept upright. The roots were then transferred to new 1/2 MS agar plates and inoculated with 10 μL of pretreated planktonic *B. subtilis* cells (prepared as described above). Plates were maintained in a static incubator at 30 °C for 1 or 5 days. Plant roots were washed 3× with 1× PBS using a shaker at 60 rpm. Samples were fixed overnight with 2.5% glutaraldehyde and washed 3× with 1× PBS. Samples were kept in the final wash until scanning electron microscopy (SEM) processing, which involved ethanol dehydration and coating (Filgen Osmium Sputter Coater OPC-60).

Results and discussion

Multiple layers of positively charged polystyrene nanoplastics are necessary to inhibit the planktonic growth of *Bacillus subtilis*

Although many studies have shown that positively charged nanoplastics bind to bacteria, the fate of these nanoplastic coatings and how non-quaternary amine (PS-NH_2)-functionalized nanobeads exert antimicrobial effects remain poorly understood. Here, we established the correlation between the degree of PS-NH_2 surface coverage and its effect on *B. subtilis* viability. We first monitored how pre-exposure to PS-NH_2 affects *B. subtilis*' planktonic growth. At PS-NH_2 concentrations below 10 μg mL^{-1}, we found that PS-NH_2 did not significantly affect *B. subtilis*; instead, we observed a slight increase in the growth rate (Fig. 1a and more growth parameters in Fig. S2†). However, as the PS-NH_2 concentration increased to 10 and 12.5 μg mL^{-1}, we observed an extended lag phase, although the exponential phase still showed a slightly elevated growth rate. Complete growth inhibition was only observed at higher concentrations (≥15 μg mL^{-1}). These results are consistent with previous studies which showed that PS-NH_2 primarily extends the lag phase of planktonic growth before reaching concentrations sufficient to completely inhibit bacterial proliferation.[19,20]

To correlate nanoplastic surface coverage with their growth-inhibiting effects, we used atomic force microscopy (AFM) to obtain high-resolution images of nanoplastic-exposed *B. subtilis* and compared this with the bacterial growth data. The high spatial resolution afforded by AFM enabled us to image the nanoplastics bound to the surface of *B. subtilis* in a liquid environment, without the need for extensive sample processing.[21] Fig. 1b are AFM images of *B. subtilis* exposed to increasing concentrations of PS-NH_2; additional images are provided in Fig. S3.† By comparing these images with the growth profiles in Fig. 1a, we can directly correlate the extent of

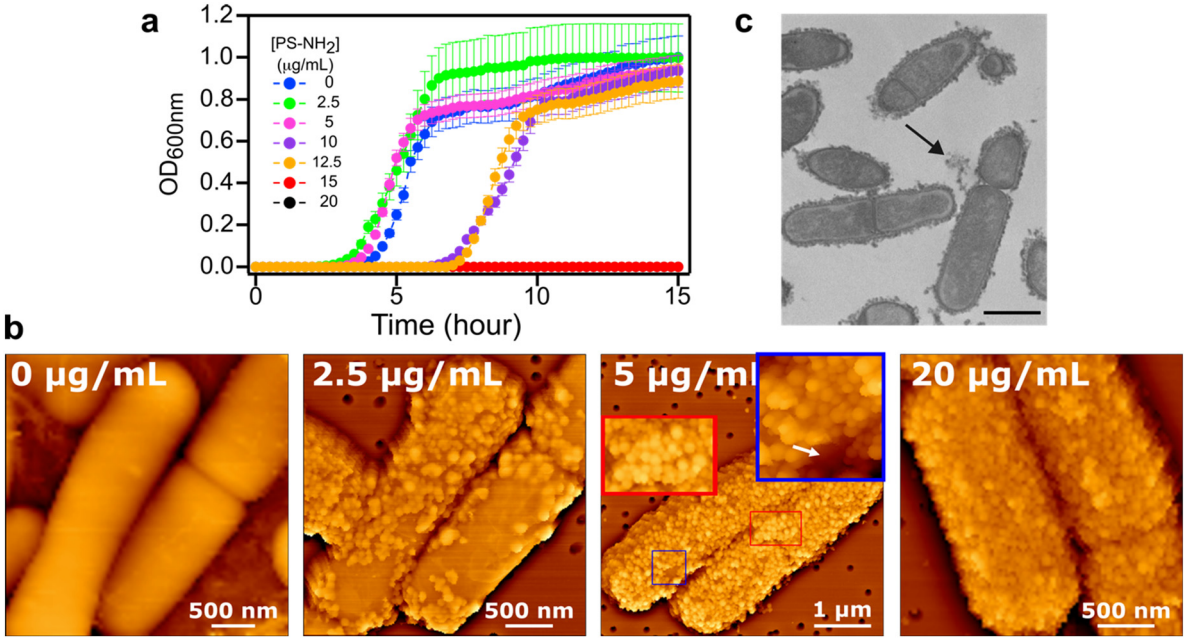

Fig. 1 Correlation between nanoplastic surface coverage and growth inhibition in *Bacillus subtilis*. (a) Planktonic growth curves (OD_{600}) of *B. subtilis* at 37 °C in LB medium after pre-treatment with PS-NH_2 at room temperature for 30 min in water. Error bars represent the standard deviation from a total of nine samples from three independent colonies. (b) Atomic force microscopy (AFM) images of *B. subtilis* after incubation with increasing concentrations (0–20 μg mL^{-1}) of PS-NH_2. Insets highlight a patch of nanoplastic-free area (blue) and areas with multiple layers of nanoplastic coating (red). At least 20 cells were imaged per nanoplastic concentration. (c) Transmission electron microscopy (TEM) image of *B. subtilis* after 30 min of incubation with PS-NH_2 in water. Black arrow points to detachment of nanoplastics from the bacterial membrane. Scalebar: 2 μm.

nanoplastic binding (*i.e.*, surface coverage) with their effects on planktonic growth. At 2.5 μg mL^{-1} of PS-NH_2, the second panel of Fig. 1b shows that nanoplastics are randomly distributed on the bacterial surface, appearing as small spherical bumps. This contrasts with the smooth surface of untreated cells (Fig. 1b, first panel). Our AFM imaging demonstrates that partial surface coverage at this concentration has minimal impact on planktonic growth.

At 5 μg mL^{-1} of PS-NH_2, where planktonic growth remains largely unaffected (Fig. 1a), we observed a near-complete surface coverage on the bacterial surface (Fig. 1b, third panel). While certain regions remain nanoplastic-free (white arrow in blue inset), multiple layers of nanoplastics have formed in other areas (red inset). This suggests that even with nearly 100% surface coverage, growth inhibition does not occur.

At PS-NH_2 concentrations of 10–12.5 μg mL^{-1}, where an extended lag phase indicated inhibited growth, our AFM imaging showed complete coverage of the bacterial surface, with multiple layers of nanoplastics present in some areas (Fig. S3†). At higher concentrations (≥15 μg mL^{-1}) that resulted in total growth inhibition, this complete surface coverage and multilayered nanoplastic coating persisted (Fig. 1b, fourth panel). We confirmed that PS-NH_2 forms a stable nanoplastic coating around *B. subtilis*, as it remained firmly attached even after 12 hours incubation in water (Fig. S4†).

Collectively, our AFM and planktonic growth assays demonstrate that *B. subtilis* can recover from exposure to positively charged nanoplastics in rich liquid media, despite the presence of stable nanoplastic coatings on its surface. We further observed that negatively charged polystyrene nanoplastics—carboxylate-, sulfate-, and non-functionalized PS—do not exhibit any biocidal activity (Fig. S5†), as previously reported for other bacteria.[22] Transmission electron microscopy (TEM) images further show that these negatively charged nanoplastics also do not bind to the surface of *B. subtilis* after 30 min exposure (Fig. S6†), suggesting that the ability of PS-NH_2 to form a stable nanomaterial coating on the bacterial surface is the primary factor behind its growth-inhibitory effects.

A multilayer PS-NH_2 coating does not directly disrupt cells or induce nanoparticle uptake

By correlating AFM images with the planktonic growth parameters of *B. subtilis*, we showed that significant accumulation of PS-NH_2 on the bacterial surface is necessary to inhibit planktonic growth. We next investigated whether this nanomaterial coating compromises the structural integrity of the bacterial envelope, which could lead to cell death and nanoparticle internalization. TEM images in Fig. 1c show that even at the highest nanoplastic concentration tested, where the bacterial surface was entirely coated with nanoplastics, the structural integrity of the cellular envelope remained intact. This observation was consistent across all nanoplastic concentrations tested (Fig. S7,† with at least 50 cells imaged per nanoplastic concentration), where the structural features of nanoplastic-bound cell envelopes resembled those of bacteria not exposed to nanoplastics (Fig. S7†). Both Fig. 1c and S7† highlight multilayer nanoplastic coatings on certain regions of

the bacterial surface (white arrows in Fig. S7†), similar to the observations made with AFM (Fig. 1b and S3†). However, we note that TEM sample preparation, being more invasive, may result in some detachment of nanoplastic coatings from the bacterial surface, as indicated by the black arrow in Fig. 1c.

Our TEM images also show that nanoplastic binding does not result in the translocation of nanoplastics into the cell interior (Fig. 1c and S7†). Even in the presence of multilayer nanoplastic coating, we observed no nanoparticles inside any of the cells. Previous research suggested that binding of PS-NH_2 could damage the cell envelope of *B. subtilis* and lead to nanoparticle internalization, but this was only observed after a 3 hour exposure.[23] Given the thick peptidoglycan layer (~30–40 nm) characteristic of the Gram-positive *B. subtilis*, with pore sizes potentially smaller than 7 nm,[24,25] the translocation of ~80–100 nm nanoplastics into their lumen cannot occur without severely damaging the cell envelope. This suggests that the previously observed nanoplastic internalization, where non-specific entry was observed, occurred due to injury in the cell envelope.[23,26–28] In our study, we found that a 30 minute incubation with PS-NH_2, resulting in the formation of a very stable nanoplastic coating, does not trigger cell envelope disruption, which could otherwise facilitate nanoparticle uptake. Our results are consistent with previous studies that showed both Gram-positive (*L. lactis*) and Gram-negative (*P. fluorescence* and *E. coli*) bacteria do not internalize commercially available ~100 nm PS-NH_2.[19,20]

B. subtilis sheds nanoplastics and forms "nanoplastic corona" before cell division resumes

Our nanoscale characterizations of *B. subtilis*–nanoplastic interactions demonstrate that even with a very dense nanoplastic

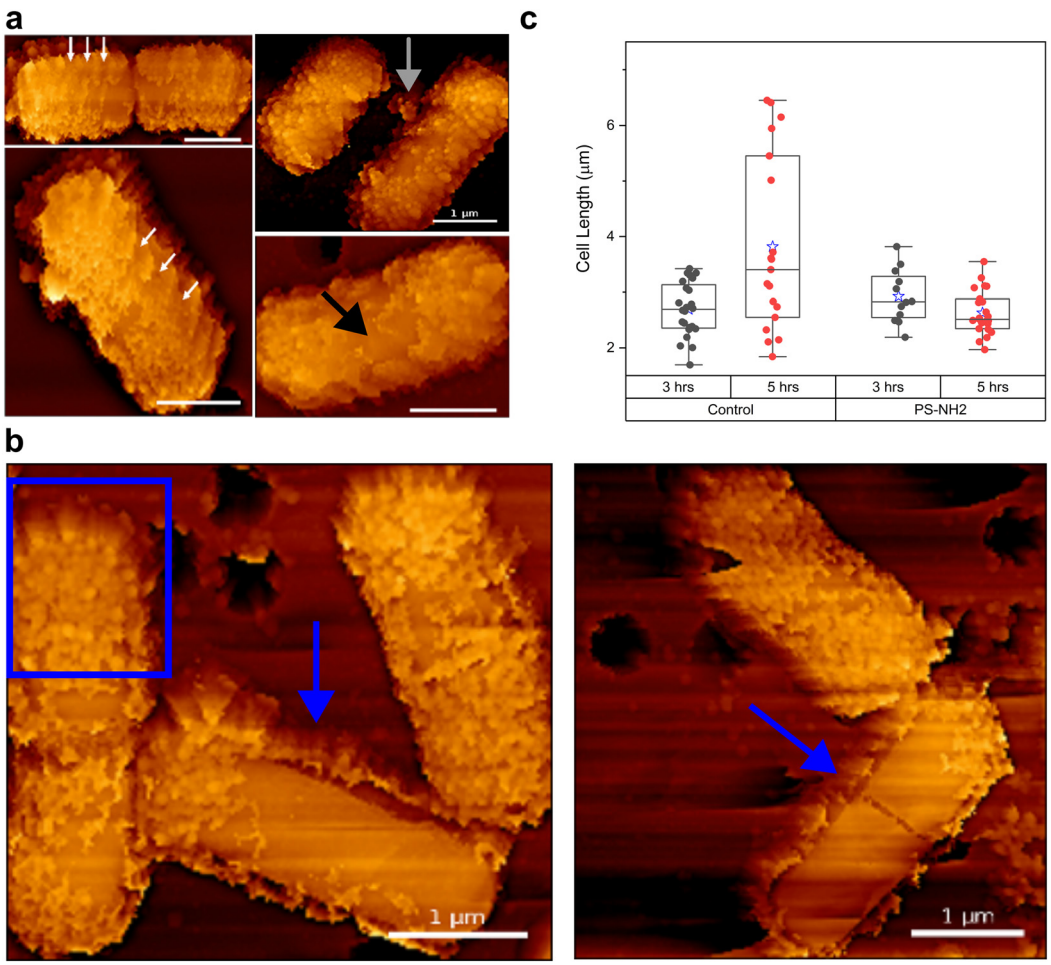

Fig. 2 AFM images of *B. subtilis* shedding nanoplastics from their surface after incubation in LB medium. (a) AFM images taken 3 h after incubation. Nanoplastic-free regions are observed near the cell division site in the middle of the cell, both without (black arrows) and with a visible septum (upper left panel). White arrows indicate nanoplastic-free regions along the cylindrical part of the cell following a helical pattern. (b) After 5 h of incubation, film of nanoplastics mixed with cellular debris (blue square) surrounds each cell, forming a "nanoplastic corona" a few nanometers away from the cell surface (blue arrows). (c) Cell length measurements of surface-immobilized *B. subtilis*, with and without a 30 minute pre-exposure to 2.5 μg mL^{-1} PS-NH_2, after 3- and 5 h of incubation in LB media at 37 °C. The blue star represents the average cell length. ANOVA analysis showed no significant difference between 3- and 5 h of growth in PS-NH_2-treated *B. subtilis*, while a significant difference (p-value < 0.001) was observed for untreated control.

coating, no signs of structural damage were observed to explain the bactericidal effects of nanoplastic exposure. We therefore investigated how nanoplastic-coated bacteria can grow in rich media despite nearly 100% of their cell surface being covered by PS-NH_2. We performed an AFM time-lapse assay to track changes in nanoplastic coating during growth. Although the bacteria were immobilized to be compatible with AFM imaging—unlike their freely floating counterparts during planktonic growth assays (Fig. 1a)—they were still grown at 37 °C in liquid media to closely mimic planktonic growth conditions (*i.e.*, growth under liquid conditions).

Fig. 2a are AFM images of nanoplastic-coated bacteria ~3 h after resuming growth conditions, showing areas clear of nanoplastics near the cell division septum (Fig. 2a, upper left panel). Even in bacteria without a visible septum, nanoplastic-free surfaces are observed near the middle of the cell (Fig. 2a black arrow). In addition, we were able to resolve helical regions of low nanoplastic density along the cylindrical part of the cell (white arrows in Fig. 2a and S8†).

Previous studies have reported that during the growth of *B. subtilis*, extensive peptidoglycan (PG) insertion occurs at the cell division site in the middle of the cell.[29–31] Newly synthesized PG is also inserted along the cylindrical part in a helical pattern.[30] During this cell wall turnover, old PG on the cell surface is hydrolyzed and replaced with newly synthesized PG.[29] Our AFM imaging suggests that this cell wall turnover contributes to the removal of nanoplastics from the cell surface (grey arrow in Fig. 2a), resulting in nanoplastic-free regions on the cell envelope. We confirmed that these nanoplastic-free regions do not result from spontaneous detachment of bound PS-NH_2, as the nanoplastic coating remained firmly attached even after 12 hours of equilibration in water, a condition in which bacteria are metabolically inactive and unable to synthesize and insert new cell wall materials (Fig. S4†).

In addition to cell wall turnover, our AFM imaging points to another mechanism by which nanoplastic-coated *B. subtilis* actively shed their nanoplastic coating. Fig. 2b shows that ~5 hours after resuming growth conditions, nanoplastics initially directly attached to the cell surface have now formed corona-like structures (*i.e.*, nanoplastic corona), surrounding the bacteria a few nanometers away from the surface (blue arrows in Fig. 2b; additional images in Fig. S9†). Within these corona structures, nanoplastics are still present, albeit with lower density, as indicated by some spherical structures embedded within the corona (Fig. 2b, blue square).

Our AFM characterization further showed that while *B. subtilis* actively remove their nanoplastic coating, there was no observable change in their cell length (Fig. 2c). In contrast, the untreated control exhibited cell elongation and cell division ~5 hours after growth conditions were resumed (Fig. 2c). We note that these changes in cell length (Fig. 2c) do not directly coincide with the characteristic growth curves shown in Fig. 1a, where no differences were observed between control and bacteria pre-exposed to 2.5 μg mL^{-1} PS-NH_2. We propose that this could be due to differences in growth conditions (*i.e.*, normal planktonic growth in liquid LB media for Fig. 1a *vs.* immobilized bacteria in liquid LB media in Fig. 2c). Such differences in growth modes can substantially alter how *B. subtilis* responds to PS-NH_2 exposure (see next section below). Nevertheless, these results suggest that while *B. subtilis* are actively removing their nanoplastic coating, cell elongation and division are suspended, which could partly explain the longer lag times observed during planktonic growth after nanoplastic exposure (Fig. 1a). Although the mechanism behind the nanoplastic removal and corona formation is still under investigation, our nanoscale characterization demonstrates that this biologically active response to nanoplastic exposure significantly impacts cell growth.

Pre-exposure to PS-NH_2 more strongly inhibits colony biofilm formation than planktonic growth in *B. subtilis*

B. subtilis, a plant growth-promoting rhizobacterium (PGPR), forms biofilms to adhere to and colonize root surfaces. Since biofilm formation on agar–air interface more closely mimic biofilm formation on root surfaces in soil (*i.e.*, root–air interface), we examined the impact of nanoplastic exposure on colony biofilm formation. We demonstrate that PS-NH_2 exposure impairs *B. subtilis*' ability to form colony biofilms (Fig. 3a). Even at the lowest nanoplastic concentrations tested (2.5 and 5 μg mL^{-1}), only small, sporadic colonies grew on agar after 24 hours (Fig. 3a, upper middle panels). These small colonies persisted for 5 days (Fig. 3a, bottom panels). Furthermore, even if colony biofilms were grown on agar containing LB supplemented with glycerol and manganese (LBGM), a medium known to promote growth of more robust biofilms,[32] pre-exposure to low concentration of PS-NH_2 (2.5 μg mL^{-1}) still inhibited colony biofilm formation (Fig. S10A†). In contrast, untreated samples and those exposed to negatively charged nanoplastics, formed complete biofilms within the same timeframe (Fig. 3a, leftmost panel and S10B,† respectively). These results highlight the stark contrast between the effects of PS-NH_2 exposure on the different modes of *B. subtilis* growth, where lower nanoplastic concentrations could already inhibit colony biofilm formation while planktonic growth in liquid LB media is barely inhibited (Fig. 3a *vs.* 1a).

To understand why colony biofilm formation at air interfaces is more inhibited by nanoplastic exposure than growth under liquid environments, we monitored the fate of the nanoplastic coating on *B. subtilis* surfaces by AFM imaging. We grew biofilms on polycarbonate (PC) membrane filters placed atop LB–agar (we have shown in our previous work that PC filters support bacterial growth and biofilm formation on agar, and are compatible with high-resolution AFM imaging).[33] Fig. 3b shows the untreated controls grown at the agar–PC–air interface, while Fig. 3c are AFM images of nanoplastic-coated bacteria. The contrast between the two is striking: after 12 hours of growth, the untreated *B. subtilis* formed densely packed, multilayer bacterial mats (Fig. 3b, bottom panel), with some

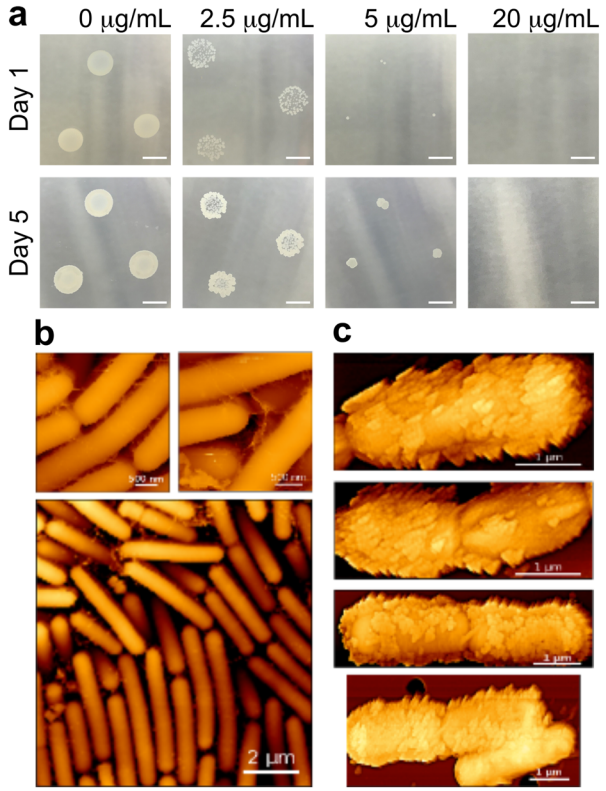

Fig. 3 Pre-exposure to PS-NH_2 is more inhibitory to colony biofilm formation. (a) Untreated colony biofilms on agar–air interface continue to grow over 5 days (left-most panels), whereas pre-exposure to 2.5 μg mL^{-1} PS-NH_2 inhibits complete biofilm formation, with only sporadic colonies forming at higher PS-NH_2 concentrations. AFM images of (b) colony biofilms formed by untreated bacteria after 12 h of growth on agar–PC membrane–air interface, while (c) the surface of PS-NH_2-treated bacteria remains covered with nanoplastics.

interspersed extracellular polymeric substances (Fig. 3b, top panel), hallmarks of biofilm formation. In contrast, the nanoplastic-coated bacteria failed to proliferate and *B. subtilis* remained as individual cells with surfaces still decorated with nanoplastics (Fig. 3c). Here, we note that growth of nanoplastic-coated bacteria at the agar–PC membrane–air interface appears to be more inhibited than at the agar–air interface, where we still observed small colony formation. This suggests in that the growth environment do heavily influence how bacteria respond to nanoplastics coating their envelope. Despite their impaired growth and proliferation, we still observed that nanoplastic-coated *B. subtilis* were still able to shed some of their nanomaterial coating. However, unlike the nanoplastic corona that formed from immobilized bacteria after only 5 hours in liquid, freeing the cell envelope of nanomaterial coating, bacteria grown at the agar–PC filter–air interface exhibited only partial nanoplastic-free regions, with patches of nanoplastic materials still directly attached to the cell envelope (Fig. 3c). This suggests that the biologically active process of removing the nanoplastic coating from the bacteria surface is heavily influenced by the bacterial growth environment (*i.e.*, liquid or air interfaces). Our high-resolution imaging suggests that growth under liquid conditions could facilitate nanoplastic removal more than air interfaces, making the physical environment (*i.e.*, root–liquid *vs.* root–air interfaces) highly consequential in determining how PGPR can survive in nanoplastic-polluted agricultural areas.

PS-NH_2 impairs *B. subtilis*' ability to colonize tomato roots

Our investigations imply that nanoplastic exposure may undermine the benefits of *B. subtilis*, which relies on colonizing and forming biofilms on plant roots—especially in traditional agricultural environments, where growth primarily occurs at root–air interfaces.[10] To test this, we assessed how pre-exposure to PS-NH_2 affects *B. subtilis*' ability to colonize tomato roots grown on Murashige and Skoog (MS) agar, mimicking the root–air interface (schematic shown in Fig. 4a). Scanning electron microscopy (SEM) images show different regions of tomato roots one and five days after inoculation with untreated *B. subtilis* (0 μg mL^{-1}) and bacteria pre-treated with low (2.5 μg mL^{-1}) and high (20 μg mL^{-1}) concentrations of PS-NH_2 (Fig. 4b). Untreated bacteria readily colonized the root surface after one day and formed extensive biofilms after five days, consistent with a prior work.[10] Except for the root cap—which consists mainly of dead root cells—bacteria were found on both the elongation and maturation regions of the root (Fig. S11†). However, pre-exposure to even a low concentration of PS-NH_2 (2.5 μg/mL) resulted in a failure to colonize the root surface; very few bacteria and no significant biofilm formation were observed even after five days (Fig. 4b and S11†). Pre-treatment with a higher concentration of 20 μg mL^{-1} nanoplastics led to a complete inability to colonize the root surface. Overall, our data strongly demonstrate that PS-NH_2 exposure can significantly hinder root binding and biofilm formation by *B. subtilis*, raising concerns about potential effects of plastic pollution in agricultural soils.

Conclusions

Although the impact of nanoplastics in aquatic environments is well-documented, their effects on terrestrial ecosystems, particularly agricultural soils, are less understood. Agricultural practices often use materials like biosolids, sludge, polymer-coated fertilizers, mulch, and plastic packaging to improve productivity. However, these materials can release nanoplastics into the soil, raising sustainability concerns due to documented negative impacts on rhizobacteria, plants and soil properties. The occurrence of nanoplastic in real environments is no longer hypothesized, as recent studies have proven their existence.[34]

Our work demonstrates that the model nanoplastic PS-NH_2, can form stable, multilayer coatings on the surface of the plant growth-promoting bacterium, *B. subtilis*. In response, the bacteria activate processes to remove nanoplastics from their surface. While the exact mechanisms behind these biological responses are still under investigation, we have shown they are heavily influenced by the bacteria's growth environment—whether at air or liquid interfaces. Using tomato plant as a

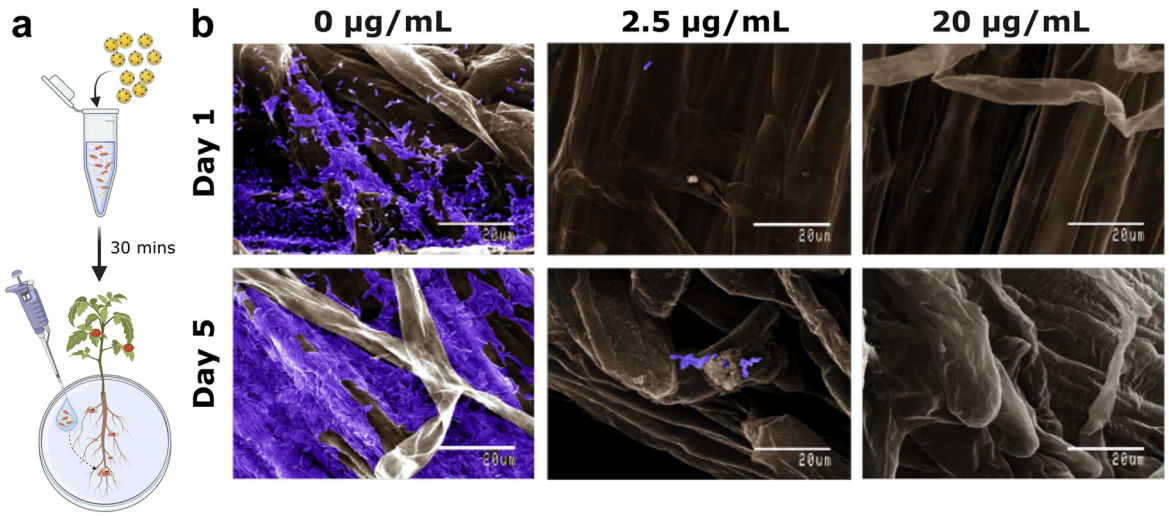

Fig. 4 Pre-exposure to PS-NH_2 inhibits *B. subtilis* colonization and biofilm formation on tomato roots. (a) Schematic outlining the experimental procedure used to inoculate tomato roots with PS-NH_2-pre-exposed *B. subtilis*. (b) Representative SEM images of root colonization assay monitored in day 1 and day 5. Purple false coloring was used to highlight the bacteria on plant root (grey).

model for rhizobacteria colonization, we show that bacterial attachment to plant roots was severely inhibited after nanoplastic exposure.

Our study raises an area of concern about the role of nanoplastics in agricultural sustainability. Microbial biofertilizers are gaining support as alternatives to conventional chemical-based fertilizers and pesticides. If nanoplastic-coated rhizobacteria cannot effectively colonize plant roots, the benefits of these sustainable farming practices may be compromised. While alternatives exist, such as soil-less systems, many countries will continue to rely on soil-based agriculture. Our data suggest that nanoplastics could be a contributing factor to the global decline in soil fertility by disrupting interactions with plant growth-promoting bacteria.

Data availability

The data supporting this article have been included as part of the ESI,† which includes the following:

- Additional atomic force microscopy (AFM) and TEM images on nanoplastic–*B. subtilis* interaction.
- Scanning electron microscopy (SEM) images of *B. subtilis* on different regions of the tomato root.
- Characterization of nanoplastics using dynamic light scattering (DLS), phase analysis light scattering (PALS), and transmission electron microscopy (TEM).
- Bacterial growth curves and growth parameters analysis.

Author contributions

F. P., N. M. A., and R. M. S. conceived and designed the study. F. P., U. T. T. H., and N. M. A. performed the experiments and analyzed the data. K. Y. provided the methodology for the root colonization assays. F. P., N. M. A., and R. M. S. drafted the manuscript. All authors contributed to the final editing and approved the submitted version.

Conflicts of interest

There are no conflicts to declare.

Acknowledgements

We thank Dr Durga Acharya and Dr Bruno Chue of the Centre for the Neurobiology of Stress, University of Toronto Scarborough for assistance in fluorescence and electron microscopy imaging.

Notes and references

1 R. Geyer, J. R. Jambeck and K. L. Law, Production, use, and fate of all plastics ever made, *Sci. Adv.*, 2017, **3**, e1700782.
2 A. A. Horton, A. Walton, D. J. Spurgeon, E. Lahive and C. Svendsen, Microplastics in freshwater and terrestrial environments: Evaluating the current understanding to identify the knowledge gaps and future research priorities, *Sci. Total Environ.*, 2017, **586**, 127–141.
3 R. Perez-Reveron, S. J. Alvarez-Mendez, J. Gonzalez-Salamo, C. Socas-Hernandez, F. J. Diaz-Pena, C. Hernandez-Sanchez and J. Hernandez-Borges, Nanoplastics in the soil environment: Analytical methods, occurrence, fate and ecological implications, *Environ. Pollut.*, 2023, **317**, 120788.
4 E. L. Ng, E. H. Lwanga, S. M. Eldridge, P. Johnston, H. W. Hu, V. Geissen and D. L. Chen, An overview of microplastic and nanoplastic pollution in agroecosystems, *Sci. Total Environ.*, 2018, **627**, 1377–1388.
5 J. Gigault, H. El Hadri, B. Nguyen, B. Grassl, L. Rowenczyk, N. Tufenkji, S. Y. Feng and M. Wiesner, Nanoplastics are neither microplastics nor engineered nanoparticles, *Nat. Nanotechnol.*, 2021, **16**, 501–507.

6 D. M. Mitrano, P. Wick and B. Nowack, Placing nanoplastics in the context of global plastic pollution, *Nat. Nanotechnol.*, 2021, **16**, 491–500.
7 R. Lehner, C. Weder, A. Petri-Fink and B. Rothen-Rutishauser, Emergence of Nanoplastic in the Environment and Possible Impact on Human Health, *Environ. Sci. Technol.*, 2019, **53**, 1748–1765.
8 C. M. Rochman, M. A. Browne, B. S. Halpern, B. T. Hentschel, E. Hoh, H. K. Karapanagioti, L. M. Rios-Mendoza, H. Takada, S. Teh and R. C. Thompson, Classify plastic waste as hazardous, *Nature*, 2013, **494**, 169–171.
9 X. Cao, C. Wang, X. Luo, L. Yue, J. C. White, Z. Wang and B. Xing, Nano- and Microplastics Increase the Occurrence of Bacterial Wilt in Tomato (Solanum lycopersicum L.), *ACS Nano*, 2024, **18**, 18071–18084.
10 T. C. G. Kibbey and K. A. Strevett, The effect of nanoparticles on soil and rhizosphere bacteria and plant growth in lettuce seedlings, *Chemosphere*, 2019, **221**, 703–707.
11 X. D. Sun, X. Z. Yuan, Y. Jia, L. J. Feng, F. P. Zhu, S. S. Dong, J. Liu, X. Kong, H. Tian, J. L. Duan, Z. Ding, S. G. Wang and B. Xing, Differentially charged nanoplastics demonstrate distinct accumulation in Arabidopsis thaliana, *Nat. Nanotechnol.*, 2020, **15**, 755–760.
12 S. Xu, C. Wu, W. B. Guo, L. Yang, R. Ji, K. Pan and A. J. Miao, Polystyrene Nanoplastics Inhibit the Transformation of Tetrabromobisphenol A by the Bacterium Rhodococcus jostii, *ACS Nano*, 2022, **16**, 405–414.
13 T. T. Awet, Y. Kohl, F. Meier, S. Straskraba, A. L. Grun, T. Ruf, C. Jost, R. Drexel, E. Tunc and C. Emmerling, Effects of polystyrene nanoparticles on the microbiota and functional diversity of enzymes in soil, *Environ. Sci. Eur.*, 2018, **30**, 11.
14 F. A. Olabemiwo, A. Hagan, M. Cham and F. M. Cohan, Two plant-growth-promoting Bacillus species can utilize nanoplastics, *Sci. Total Environ.*, 2024, **907**, 167972.
15 S. Arnaouteli, N. C. Bamford, N. R. Stanley-Wall and A. T. Kovacs, Bacillus subtilis biofilm formation and social interactions, *Nat. Rev. Microbiol.*, 2021, **19**, 600–614.
16 H. Massalha, E. Korenblum, S. Malitsky, O. H. Shapiro and A. Aharoni, Live imaging of root-bacteria interactions in a microfluidics setup, *Proc. Natl. Acad. Sci. U. S. A.*, 2017, **114**, 4549–4554.
17 Y. M. H. Liu, D. Patko, I. Engelhardt, T. S. George, N. R. Stanley-Wall, V. Ladmiral, B. Ameduri, T. J. Daniell, N. Holden, M. P. MacDonald and L. X. Dupuy, Plant-environment microscopy tracks interactions of Bacillus subtilis with plant roots across the entire rhizosphere, *Proc. Natl. Acad. Sci. U. S. A.*, 2021, **118**, e2109176118.
18 O. Pikuda, E. G. Xu, D. Berk and N. Tufenkji, Toxicity Assessments of Micro- and Nanoplastics Can Be Confounded by Preservatives in Commercial Formulations, *Environ. Sci. Technol. Lett.*, 2018, **6**, 21–25.
19 T. Nomura, E. Fujisawa, S. Itoh and Y. Konishi, Comparison of the cytotoxic effect of polystyrene latex nanoparticles on planktonic cells and bacterial biofilms, *J. Nanopart. Res.*, 2016, **18**, 157.
20 T. Nomura, Y. Kuriyama, H. Tokumoto and Y. Konishi, Cytotoxicity of functionalized polystyrene latex nanoparticles toward lactic acid bacteria, and comparison with model microbes, *J. Nanopart. Res.*, 2015, **17**, 105.
21 Y. F. Dufrene, Atomic Force Microscopy in Microbiology: New Structural and Functional Insights into the Microbial Cell Surface, *mBio*, 2014, **5**, 01363-14.
22 M. Zajac, J. Kotynska, G. Zambrowski, J. Breczko, P. Deptula, M. Ciesluk, M. Zambrzycka, I. Swiecicka, R. Bucki and M. Naumowicz, Exposure to polystyrene nanoparticles leads to changes in the zeta potential of bacterial cells, *Sci. Rep.*, 2023, **13**, 9552.
23 S. Dai, R. Ye, J. X. Huang, B. Q. Wang, Z. M. Xie, X. W. Ou, N. Yu, C. Huang, Y. J. Hua, R. H. Zhou and B. Tian, Distinct lipid membrane interaction and uptake of differentially charged nanoplastics in bacteria, *J. Nanobiotechnol.*, 2022, **20**, 191.
24 E. J. Hayhurst, L. Kailas, J. K. Hobbs and S. J. Foster, Cell wall peptidoglycan architecture in *Bacillus subtilis*, *Proc. Natl. Acad. Sci. U. S. A.*, 2008, **105**, 14603–14608.
25 L. Pasquina-Lemonche, J. Burns, R. D. Turner, S. Kumar, R. Tank, N. Mullin, J. S. Wilson, B. Chakrabarti, P. A. Bullough, S. J. Foster and J. K. Hobbs, The architecture of the Gram-positive bacterial cell wall, *Nature*, 2020, **582**, 294–297.
26 J. R. Morones, J. L. Elechiguerra, A. Camacho, K. Holt, J. B. Kouri, J. T. Ramírez and M. J. Yacaman, The bactericidal effect of silver nanoparticles, *Nanotechnology*, 2005, **16**, 2346–2353.
27 Y. N. Slavin, K. Ivanova, J. Hoyo, I. Perelshtein, G. Owen, A. Haegert, Y. Y. Lin, S. LeBihan, A. Gedanken, U. O. Häfeli, T. Tzanov and H. Bach, Novel Lignin-Capped Silver Nanoparticles against Multidrug-Resistant Bacteria, *ACS Appl. Mater. Interfaces*, 2021, **13**, 22098–22109.
28 E. Sawosz, A. Chwalibog, J. Szeliga, F. Sawosz, M. Grodzik, M. Rupiewicz, T. Niemiec and K. Kacprzyk, Visualization of gold and platinum nanoparticles interacting with *Salmonella enteritidis* and *Listeria monocytogenes*, *Int. J. Nanomed.*, 2010, **5**, 631–637.
29 D. J. Scheffers and M. G. Pinho, Bacterial cell wall synthesis: New insights from localization studies, *Microbiol. Mol. Biol. Rev.*, 2005, **69**, 585–607.
30 R. A. Daniel and J. Errington, Control of cell morphogenesis in bacteria: Two distinct ways to make a rod-shaped cell, *Cell*, 2003, **113**, 767–776.
31 D. H. Edwards, H. B. Thomaides and J. Errington, Promiscuous targeting of *Bacillus subtilis* cell division protein DivIVA to division sites in Escherichia coli and fission yeast, *EMBO J.*, 2000, **19**, 2719–2727.
32 M. Shemesh and Y. Chai, A combination of glycerol and manganese promotes biofilm formation in *Bacillus subtilis* via histidine kinase KinD signaling, *J. Bacteriol.*, 2013, **195**, 2747–2754.

33 C. T. Kreis and R. M. A. Sullan, Interfacial nanomechanical heterogeneity of the *E. coli* biofilm matrix, *Nanoscale*, 2020, **12**, 16819–16830.

34 A. Wahl, C. Le Juge, M. Davranche, H. El Hadri, B. Grassl, S. Reynaud and J. Gigault, Nanoplastic occurrence in a soil amended with plastic debris, *Chemosphere*, 2021, **262**, 127784.